THE ASTROPHYSICAL JOURNAL, 314:457–475, 1987 March 15

H I MAPS OF S0 GALAXIES WITH POLAR RINGS

J. H. VAN GORKOM
Princeton University and National Radio Astronomy Observatory
PAUL L. SCHECHTER
AND
JEROME KRISTIAN
Mount Wilson and Las Campanas Observatories, Carnegie Institution of Washington
Received 1986 May 12; accepted 1986 September 2

ABSTRACT

VLA maps in the 21 cm line of neutral hydrogen have been obtained for three S0 galaxies with polar rings, and an upper limit on H I has been obtained for a fourth system. Polar rings span a continuum, ranging from those in which the H I seems to be in a relatively stable configuration, producing stars throughout its extent, to those in which the H I is very asymmetric, with stars forming only at the inner edge of an H I disk. A deep CCD image of MGC −5-7-1 shows arcs and filaments, some of which coincide with the likewise chaotic H I. If the system formed as the result of the merger of a gas-rich system with an S0 galaxy, the gas-rich system must have included considerable numbers of stars.

Subject headings: galaxies: internal motions — galaxies: structure — radio sources: 21 cm radiation

I. INTRODUCTION

Polar ring galaxies are unusual in that their stars and gas orbit in two distinct, roughly orthogonal planes. Such configurations strike one as unlikely first, because they would appear to be unstable to disruption by differential precession, and second, because of the difficulty in explaining how such a configuration might have arisen as part of the collapse of a single, coherent object.

If they are not unstable to differential precession, their potentials must deviate from axisymmetry in a way which may bear on the potentials of more ordinary galaxies. And if they did not form as part of a coherent collapse, perhaps ordinary galaxies likewise formed less coherently than we are inclined to think.

The issues of stability and formation are related. If the time scales for the disruption of polar rings are short, they must have formed recently. If, as has been argued, polar rings form by the accretion of gas-rich companions, the frequency of such events computed from the statistics of polar rings will be inversely proportional to their assumed lifetimes.

How stable are polar rings? By what mechanism and how recently did they form? With these and related issues in mind, we obtained VLA observations in the 21 cm line of neutral hydrogen of four previously unmapped polar rings. Low-resolution maps were produced for three systems, and an upper limit was obtained for the fourth. The two most interesting systems were subsequently mapped with higher resolution. CCD images for one of the systems were obtained at Las Campanas.

We present some background on polar rings in § II. Details of our observations and reduction procedures are described in § III. Results from the observations, in the form of total hydrogen contours, mean velocity maps, position-velocity diagrams, and channel maps are presented in §§ IV–VII. We discuss each galaxy in turn, starting with the least interesting and proceeding to the most interesting. In § VIII we discuss polar rings as a group and address the questions of stability, age, and formation mechanism.

II. BACKGROUND

a) Observations

Schweizer, Whitmore, and Rubin (1983) present a list of 22 galaxies they consider candidates for classification as S0's with polar rings. Their Figure 2 shows photographs of eight such systems, including the familiar "Spindle" galaxy NGC 2685.

Long-slit absorption-line rotation curves have been obtained for the central S0 components of three systems: NGC 2685 (Schechter and Gunn 1978), A0136−0801 (Schweizer, Whitmore, and Rubin 1983), and NGC 4650A (Schechter, Ulrich, and Boksenberg 1984). In each case the central component would appear to be rotating about its short axis, with a high ratio of rotation velocity to central stellar-velocity dispersion, consistent with the interpretation that one is seeing an edge-on S0 galaxy.

The ring around NGC 4650A is ragged and knotty (Laustsen and West 1980), which might be taken as an indicator of youth. Its central S0 has strong Balmer absorption lines (Schechter, Ulrich, and Boksenberg 1984), another signature of recent star formation, and one not usually found in S0 galaxies. It would seem that some of the material associated with the ring has found its way to the center of the S0.

Neutral hydrogen observations have been obtained for three systems. In two of these, II Zw 73 and UGC 7576, Schechter *et al.* (1984) found that the H I emission coincided almost exactly with the optical image of the polar ring, indicating that the rings are relatively stable and have had time to form significant numbers of stars throughout. However, they also found large ratios of neutral hydrogen to optical luminosity in the two systems they studied, indicating either their relative youth or that star formation in such systems has been relatively inefficient.

The hydrogen distribution in NGC 2685 is complex (Shane 1980). There are evidently two H I systems, an inner one corresponding to the optical filaments and orbiting close to the pole of the S0, and an outer one corresponding to a faint optical ring, in a plane close to that of the central S0.

b) Theory

Since there are several cases of rings which appear to lie a few tenths of a radian from the pole of the S0, one might suppose that such rings are unstable to disruption by differential precession in the (presumably oblate) potential of the underlying S0 (Tohline, Simonson, and Caldwell 1982; Richstone and Potter 1982). However, if one admits the possibility that such systems might be embedded within slowly tumbling triaxial potentials, it might in some cases prove possible to construct equilibrium models (van Albada, Kotanyi, and Schwarzschild 1982). However, this mechanism is ruled out in the case of NGC 4650A, since the gas in the ring and the stars in the S0 rotate in the same sense about the pole of the S0.

Sparke (1986) has argued that the hydrogen masses in II Zw 73 and UGC 7576 may be large enough to stabilize their rings against differential precession. These results depend critically on the width of the ring, with the self-gravitating equilibria exhibiting warps which increase as the cube of the difference between the inner and outer radii. The required ranges of radius, while smaller than those estimated by Schechter *et al.* (1984), are not unreasonably so.

III. OBSERVATIONS AND DATA REDUCTION

a) H I Observations with the C-D Array

The first series of H I observations was carried out with the Very Large Array (VLA) in its most compact D configuration. Two galaxies at low declinations were observed with an extended (3 km) north arm, which yielded a rounder beam. Since the program was of an exploratory nature, a large velocity range was covered (1000 km s^{-1}), and consequently only a modest velocity resolution (40 km s^{-1}) could be used. The instrumental parameters of the observations are summarized in Table 1*a*. A description of the VLA is given by Thompson *et al.* (1980). An on-line Hanning smoothing in velocity was applied to the data. Following this smoothing, every other channel was discarded, leaving a set of independent channels, for which the velocity resolution is equal to the channel spacing. The dropping of channels was done to circumvent VLA software restrictions in effect at the time the data were taken, which placed limits on the numbers of frequency channels and baselines that could be used.

Standard VLA calibration procedures were used, maps were made on the "pipeline," and further analysis of the maps was

TABLE 1A

INSTRUMENTAL PARAMETERS OF THE LOW-RESOLUTION VLA OBSERVATIONS

PARAMETER	SOURCE			
	NGC 4650A	MCG −5-7-1	A0136−0801	IC 1689
Array	C-D	C-D	D	D
Observing dates	1984 Jul 12	1984 Jul 14	1984 Aug 2	1984 Aug 2
Duration of observations (hr)	4	4	4	4
Total number of antennas	25	25	25	25
Shortest, longest spacing (*m*)	40, 3000	40, 3000	40, 1000	40, 1000
Field center (1950)	$\alpha = 12^h42^m04^s.6$	$02^h26^m12^s.0$	$01^h36^m00^s$	$01^h20^m57^s.0$
	$\delta = -40°26'27''$	$-32°06'03''$	$08°01'00''$	$32°47'28''$
Half-power of primary beam (′)	30	30	30	30
Half-power of synthesized beam (″)	40 × 30, PA 27°.6	72 × 41, −7°	74 × 56, 2°.6	68 × 56, 81°.2
Velocity of band center, heliocentric (km s^{-1})	2910	4625	5528	4700
Number of velocity channels	31	31	31	31
Velocity channel spacing (≡ velocity resolution) km s^{-1}	42.0	42.5	42.75	42.5
RMS noise in channel maps (mJy per beam)	1.3	0.6	0.6	0.6
Equivalent T_b for 1.0 mJy per beam area (K)	0.55	0.22	0.16	0.2

TABLE 1B

INSTRUMENTAL PARAMETERS OF THE HIGH-RESOLUTION VLA OBSERVATIONS

PARAMETER	SOURCE	
	NGC 4650A	MCG −5-7-1
Array	B-C	B-C
Observing dates	1985 Jun 30, Jul 4	1985 Jul 3, 4, 6
Duration of observations (hr)	3.5, 3.5	4.5, 4.5, 4.5
Total number of antennas	25	25
Shortest, longest spacing (*m*)	100, 6900	100, 6900
Number of velocity channels	31	31
Velocity channel spacing (km s^{-1})	21	21.25
Final Maps		
Half power of synthesized beam (″)	20 × 20	30 × 30
Velocity resolution (km s^{-1})	21	42.5
RMS noise per synthesized beam (mJy per beam area)	1.1	0.5
Equivalent T_b for 1.0 mJy per beam area (K)	1.6	0.7

done with NRAO's imaging processing system (AIPS) on a VAX 11/780. First, maps were made using natural weighting, in which each measured point in the UV plane gets equal weight. This optimizes sensitivity, but results in a broad synthesized beam, since the low spatial frequencies are more densely sampled at the VLA. These maps were visually inspected after subtraction of the average of all channels as a first-order attempt to remove the radio continuum emission. Only one galaxy, NGC 4650A, showed strong H I emission; two other galaxies were detected, but their emission was very weak. The fourth galaxy, IC 1689, was not detected. For NGC 4650A new maps were made using uniform weighting, with each grid cell in the UV plane getting equal weight. The resulting synthesized beam was smaller, but the noise was higher by more than a factor of 2.

For each galaxy a proper radio continuum map was constructed by taking an average of the line-free channels. The average maps were CLEANed, using the algorithm developed by Högbom (1974). The numbers of channels included in the average were, respectively, 15, 10, 16, and 24, for NGC 4650A, MCG −5-7-1, A0136−0801, and IC 1689. None of the galaxies was detected in the continuum, at 3 σ upper limits which were typically 1.5 mJy per beam. The dirty continuum maps were subtracted from the line channels to remove field sources and their instrumental responses. The resulting line maps which showed H I emission were CLEANed.

Two of the galaxies were observed over frequency ranges which included 1400 MHz. The VLA generates a strong interfering signal at this frequency. As a consequence one channel in the observations of IC 1689, at 4402 km s^{-1}, could not be used. Two channels in the observations of MGC −5-7-1 were also affected. The corresponding velocities, at 4413 and 4370 km s^{-1}, are just outside the H I range.

For each galaxy an area of roughly one square degree was mapped. In the field of IC 1689 no H I emission was detected. The 5 σ detection limit of H I column density is 5×10^{19} atoms cm^{-2} per 42 km s^{-1} channel for a 68×56 arcsec^2 beam. The upper limit on the total hydrogen mass for IC 1689 given in Table 2 is derived by assuming a velocity width of 300 km s^{-1} and assuming that the H I extent in any given channel is not larger than the beam. A 3 σ upper limit and a Hubble constant of 100 km s^{-1} Mpc^{-1} were adopted.

For the other galaxies the line maps were integrated over the region of H I emission to obtain the global H I profiles shown below in Figures 5, 10, and 14. To our knowledge these are the first H I observations of these galaxies. In the field of MCG −5-7-1 an uncataloged dwarf was detected in the hydrogen at $\alpha = 02^h25^m07^s.7$, $\delta = -31°55'09''$, and 17'.5 to the NW, at a redshift of 4530 ± 20 km s^{-1}. H I distribution maps and velocity fields were derived by displaying individual maps and tracing the boundaries of the emission regions and calculating the zeroth and first moments of the profiles inside those boundaries.

b) *Observations in the B-C Array*

The maps obtained for NGC 4650A and MCG −5-7-1 were intriguing and prompted us to obtain a second series of observations with higher angular and velocity resolution. Apart from the higher resolution, the observing procedures and data reduction were identical to those used for the first series of observations.

Initial maps were produced using only the high-resolution data. The results for NGC 4650A were satisfactory, and only the high-resolution data are presented here. The data for MCG −5-7-1 suffered from the lower sensitivity of the B-C array. They were therefore degraded to the velocity resolution of the C-D observations, and both were combined in the UV plane. Natural weighted maps were then made. The results for MCG −5-7-1 are derived from these combined data, with the exception of the position-velocity profile which was derived from the higher velocity resolution data. Masks for the construction of H I distribution maps and velocity fields were created by smoothing the data cubes both spatially and in velocity to half-resolution. Cutoffs of 1 mJy per beam for NGC 4650A and 0.7 mJy per beam for MCG −5-7-1 were then adopted, eliminating those pixels with low emission in the smoothed data cubes. The H I distributions and mean velocity maps presented below were computed by applying these masks to the original unsmoothed data.

Parameters for the observations for the B-C hybrid array are given in Table 1*b*.

c) *New Optical Data*

Over the course of the last few years we have obtained new optical observations and, in some instances, made new measurements from older observations.

Newly measured positions, either from Palomar Sky Survey prints or SRC *J* survey films, accurate to ±2″, are given in Table 2. Spectra have been obtained for IC 1689 (at KPNO, using the cryogenic camera) and MCG −5-7-1 (at Las Campanas, using Shectman's Reticon spectrometer), which yielded the redshifts given for these objects in Table 2.

TABLE 2

MISCELLANEOUS DATA

	IC 1689	A0136−0801	NGC 4650A	MCG −5-7-1
cz (km s^{-1})	4567	5528[a]	2910[b]	4604
α	$01^h20^m58^s.9$	$01^h36^m25^s.4$	$12^h42^m04^s.8$	$02^h26^m11^s.5$
δ	+32°47′41″	−08°01′14″	−40°26′35″	−32°06′14″
P.A. (S0)	16°	51°.5[a]	162°	17°.3
P.A. (ring)	163°	138°[a]	60°	94°.2
i (ring)	51°	79°[a]	85°	68°
r (ring)	5″	10–32″[a]	43″[c]	20″
m	14.8	17.1[a]	14.33[d]	15.16[e]
Type	B (Zwicky)	B (total)	P (total)	B (31'.21)
Ring/total	$\lesssim$0.10	$\lesssim$0.50[a]	$\lesssim$0.3	$\lesssim$0.05
H I ($10^8 M_\odot$)	<3	8.3	26	18

REFERENCES.—(a) Schweizer, Whitmore, and Rubin 1983; (b) Schechter, Ulrich, and Boksenberg 1984; (c) Laustsen and West 1980; (d) Sersic 1967; (e) Lauberts 1984.

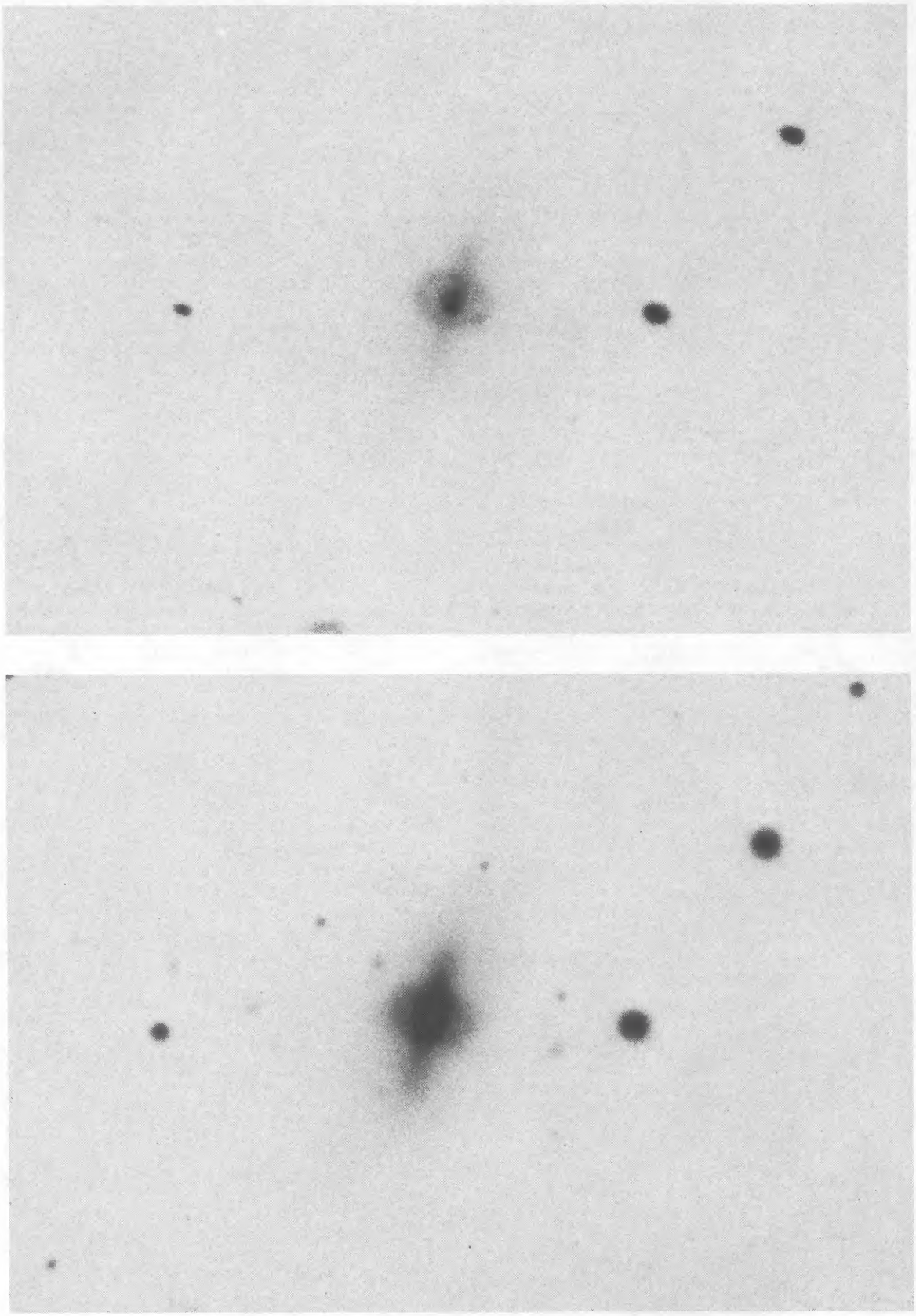

FIG. 1.—*Upper panel:* IC 1689, reproduced from a 2 hr exposure on IIIa-J emulsion obtained with a UG 2 filter at the prime focus of the Mayall telescope at Kitt Peak. *Lower panel:* IC 1689 reproduced from a 1 hr exposure on IIIa-F emulsion obtained with an RG 610 filter on the 4 m telescope.

A 30 minute exposure of MCG −5-7-1 was obtained with a Gunn *r* filter (Thuan and Gunn 1976) using a Texas Instruments 800 × 800 CCD at the Cassegrain focus of the du Pont 2.5 m telescope on Las Campanas. This yielded the position angles for the ring and S0 and the angular size and inclination for the ring given in Table 2, as well as axial ratios for the two components.

Position angles for the ring and S0 components of IC 1689 and the inclination of the ring to the line of sight were computed by tracing the two components using a trackball on the IPPS image processing system at KPNO. The digital image was kindly supplied by K. M. and S. E. Strom.

Apparent magnitudes have been assembled from the available literature and are presented in Table 2. We have made crude "eyeball" estimates for the fractional contribution of the ring to the total optical luminosity, which we also give in Table 2.

IV. IC 1689

IC 1689 was first identified as a polar ring system by Strom (private communication, 1982). Figure 1 is reproduced from a pair of plates obtained with the Kitt Peak 4 m telescope (MP 1806 and 2217), taken by S. E. and K. M. Strom as part of their study of the photometric properties of elliptical and S0 galaxies in clusters, and kindly supplied by them for publication here. The ring shows up more clearly in the photographic *U* band (*upper panel*) than in the photographic *R* band (*bottom panel*) indicating that the ring is substantially bluer than the underlying S0.

While the ring is relatively faint, there are reasons why one might hope to detect it in H I. Its blue color would argue for its relatively recent formation. The outer isophotes are slightly twisted (C. R. Lynds, private communication), which might indicate a recent encounter with an object massive enough to have distorted the S0. And there is weak [O III] emission in the nucleus (Schechter and Ulrich, in preparation), demonstrating that the system is not entirely free of gas.

If we attempt a crude decomposition of the galaxy into its S0 and polar ring components, we can estimate the amount of H I which might be expected to be associated with the ring. Taking the ring to be 2.5 mag fainter than the S0, assuming $M_H/L_B = 1$ (less than is observed in II Zw 73 and UGC 7576), and adopting, for the sake of consistency, a Hubble constant $H_0 = 100$ km s^{-1} Mpc^{-1}, we would predict an H I mass of $3.9 \times 10^8 M_\odot$.

Inspection of the channel maps obtained at this position yielded no obvious detection at 21 cm. An upper limit on the hydrogen mass associated with the ring can be obtained by assuming that the H I extent in any given channel is not larger than the beam. The optical diameter of the ring is considerably smaller than this. Assuming a velocity width of 300 km s^{-1} then yields an upper limit of $3 \times 10^8 M_\odot$ of H I, a value slightly smaller than our crude prediction. By contrast, the H I detected in MCG −5-7-1 (see § VII below) exceeds the amount predicted in a similar calculation by an order of magnitude.[1]

[1] In the time since our observation of IC 1689, R. Giovanelli (private communication) has obtained a better upper limit of $1.1 \times 10^8 M_\odot$ with the 305 m Arecibo telescope.

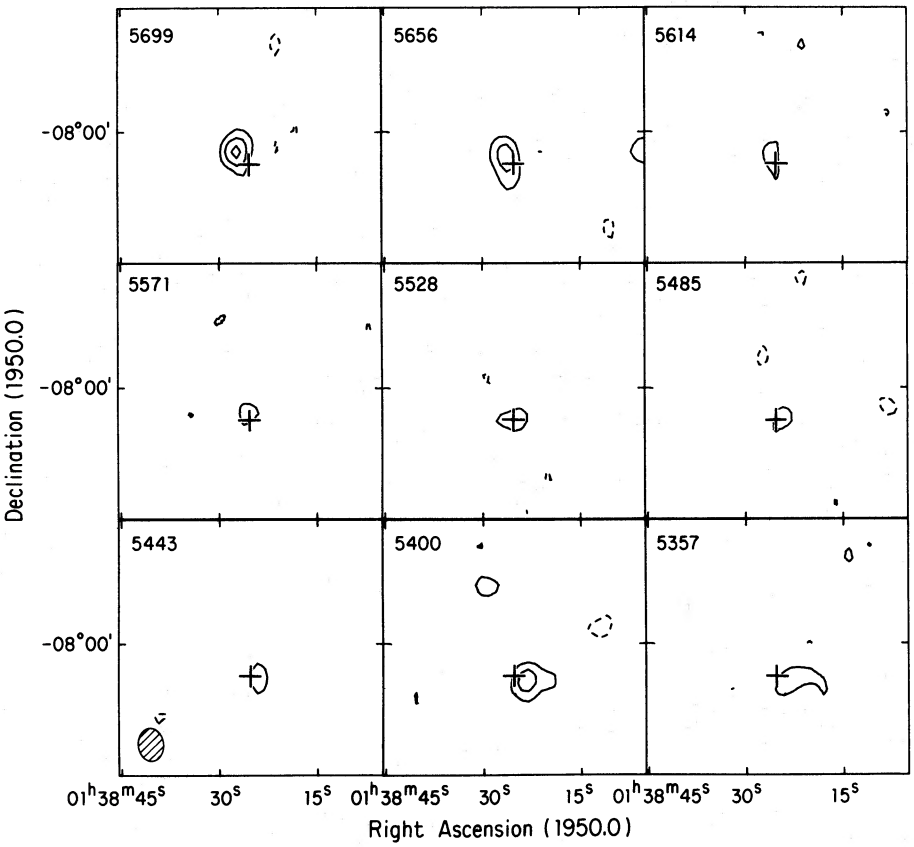

FIG. 2.—Channel maps for A0136−0801, with contours of 1.5 mJy per beam

V. A0136−0801

A photograph of this system has been published by Schweizer, Whitmore, and Rubin (1983). Neutral hydrogen is clearly evident in the channel maps, some of which are shown in Figure 2. Although the H I is not resolved in most of the channel maps, a hint of a warp to the southwest can be seen at a velocity of 5357 km s^{-1}. The separation between H I centroids at the extreme velocities is 1′, in good agreement with the optical extent of the ring. Total hydrogen contours, superposed on a photograph kindly supplied by F. Schweizer, are shown in Figure 3.

The H I is closely aligned with the major axis of the outer ring. It is unresolved in the direction of the minor axis. Therefore, all the velocity information about the system is contained in the position-velocity profile along the major axis, shown in Figure 4. The rotation velocity of 170 km s^{-1} derived from that profile agrees well with the optical emission-line rotation curve obtained by Schweizer *et al.* (1983). Since the optical observations have higher resolution, and since the H I and optical emission are similar in extent, our results add no new information about the kinematics of the system.

A global H I profile is shown in Figure 5. The total hydrogen mass, obtained by integrating the global profile over velocity, is $8.3 \times 10^8\ M_\odot$, which is a factor of 70 larger than the estimate by Schweizer, Whitmore, and Rubin (1983), based on the absorption of light from the central component by material in the ring.

This system is very much like the systems mapped by Schechter *et al.* (1984), UGC 7576 and II Zw 73, in that the observed H I appears to coincide rather closely with the optical image of the polar ring. The implication of this observation would be that however the system formed, it has had ample time for the ring to settle into an equilibrium configuration and to form stars throughout its extent. We note, however, that Schweizer, Whitmore, and Rubin (1983) argue, from their observations of dust in the ring projected onto the central S0, that the polar ring must extend beyond its optical image.

A0136−0801 is similar to the galaxy II Zw 73 (and different from the other three galaxies observed) in that the optical emis-

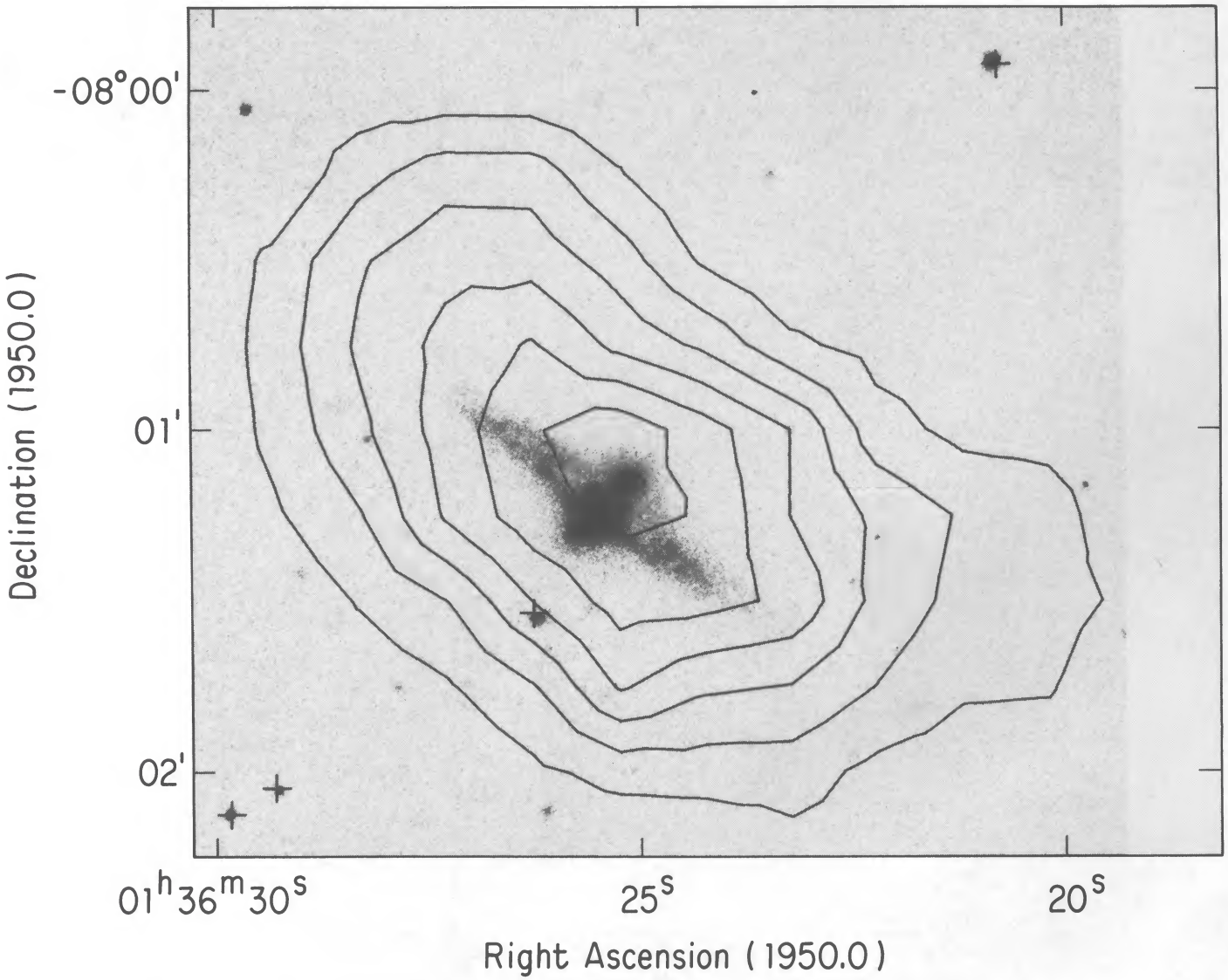

FIG. 3.—Hydrogen contours for A0136−0801, superposed on a reproduction of a 60 minute exposure on IIIa-J emulsion obtained through a GG 385 filter at the prime focus of Cerro Tololo 4 m telescope. Contours are in steps of 2.8×10^{19} atoms cm^{-2}.

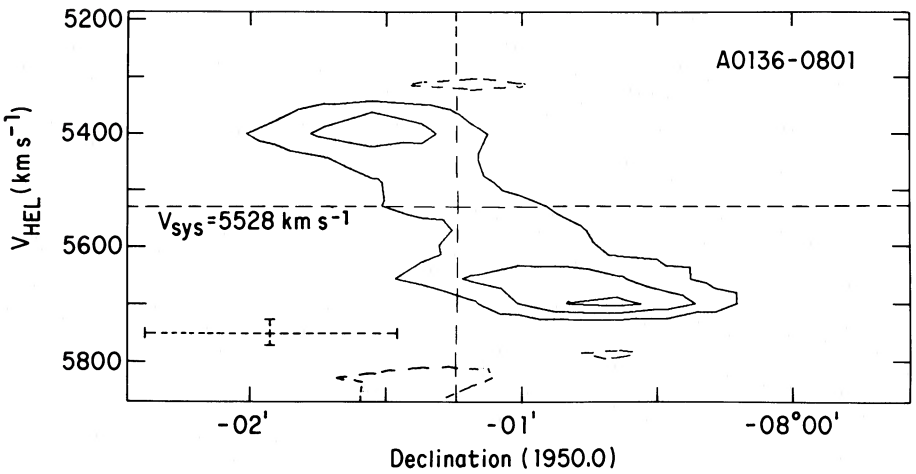

FIG. 4.—Position-velocity diagram for A0136−0801

sion from the polar ring extends over a large range of radius, with an inner edge one-third the size of the outer edge. The disk of this system looks very much like the disk of an ordinary Sb or Sc galaxy; it is the central gap and the peculiar orientation of the central, S0-like component which make the galaxy unusual.

In their discussion of this object, Schweizer, Whitmore, and Rubin (1983) emphasized the importance of polar rings as indicators of secondary events in the formation of galaxies. We would fault them only for timidity in their choice of words. The polar ring dominates the light from the system, and were the ring and central components parallel, would probably be the determining factor in its morphological classification. The ring is secondary only in that it is hard to imagine how two separate disks could have formed in a "coherent" formation scenario, and would therefore seem to have formed only after the gas in the central S0 had been exhausted or removed.

VI. NGC 4650A

Several photographs of this system have been published by Laustsen and West (1980). Neutral hydrogen is clearly evident in the channel maps, which are shown in Figure 6. Total hydrogen contours are displayed in Figure 7, superposed on a photograph kindly supplied by K. Wakamatsu. The original plate was obtained with a GG 385 filter and IIIa-J emulsion using the CTIO 4 m telescope. Figure 8 shows contours of constant heliocentric velocity. These were produced using a circular beam 20″ in diameter. A position-velocity diagram, computed by projecting the data cube onto the major axis of the polar ring, is shown in Figure 9. A position angle of −22° was adopted for the major axis. The rotation velocity derived from this diagram is 100 km s^{-1}. A global H I profile is shown in Figure 10.

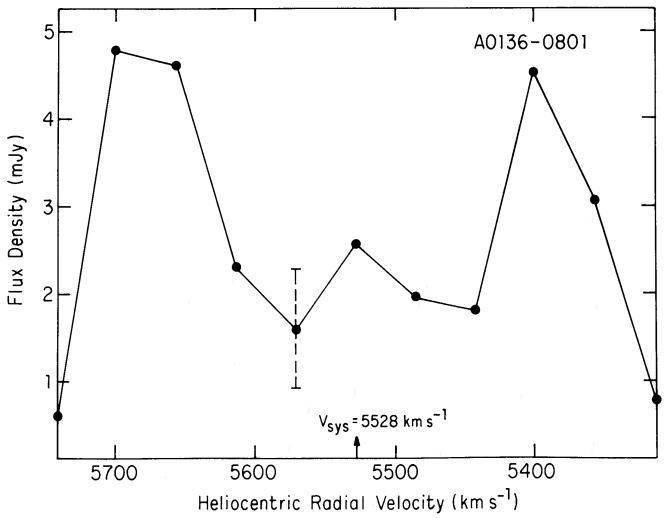

FIG. 5.—Global H I profile for A0136−0801

There is considerable structure both in the H I map and in the position-velocity diagram. As in the cases of II Zw 73 and UGC 7576, there is a minimum in the H I near the center of the system, but unlike those two cases, the minimum shows a significant offset to the north. We take the minimum to indicate that the H I is truly a ring or an annulus, and not a disk. An infinitely narrow ring would produce a linear position-velocity diagram. The deviation from linearity observed in the inner part of NGC 4650A would indicate that the hole in the H I distribution is no larger than 30″.

The H I in NGC 4650A twists on the plane of the sky, following and then extending beyond the twists observed in the optical ring. The H I first twists toward the pole of the S0, then twists away from it. The hydrogen is very asymmetric, indicating that the distribution of H I within the ring is far from uniform. The inner H I contours are considerably flatter than the outer ones, which we take as evidence that the inner parts of the ring are more nearly edge-on than are the outer parts.

The velocity field map, Figure 8, is roughly symmetric about a velocity of 2895 km s^{-1}, with the line of symmetry significantly displaced to the north of the optical position. The mean of the extreme velocities in the position-velocity diagram, 2910 km s^{-1}, agrees well with the optical velocity of the S0 galaxy. But the contour at 2910 km s^{-1} is displaced yet farther to the north. There is a significant deviation from a flat rotation curve along the northern half of the position-velocity diagram, with the velocity dropping by roughly 20 km s^{-1} at 1.′5 from the center of the galaxy, perhaps rising again farther out. This inflection occurs roughly at the point at which the H I reverses the direction of its twisting.

The optical ring in NGC 4650A is knotty and distorted, with prominent H II regions indicating significant recent star forma-

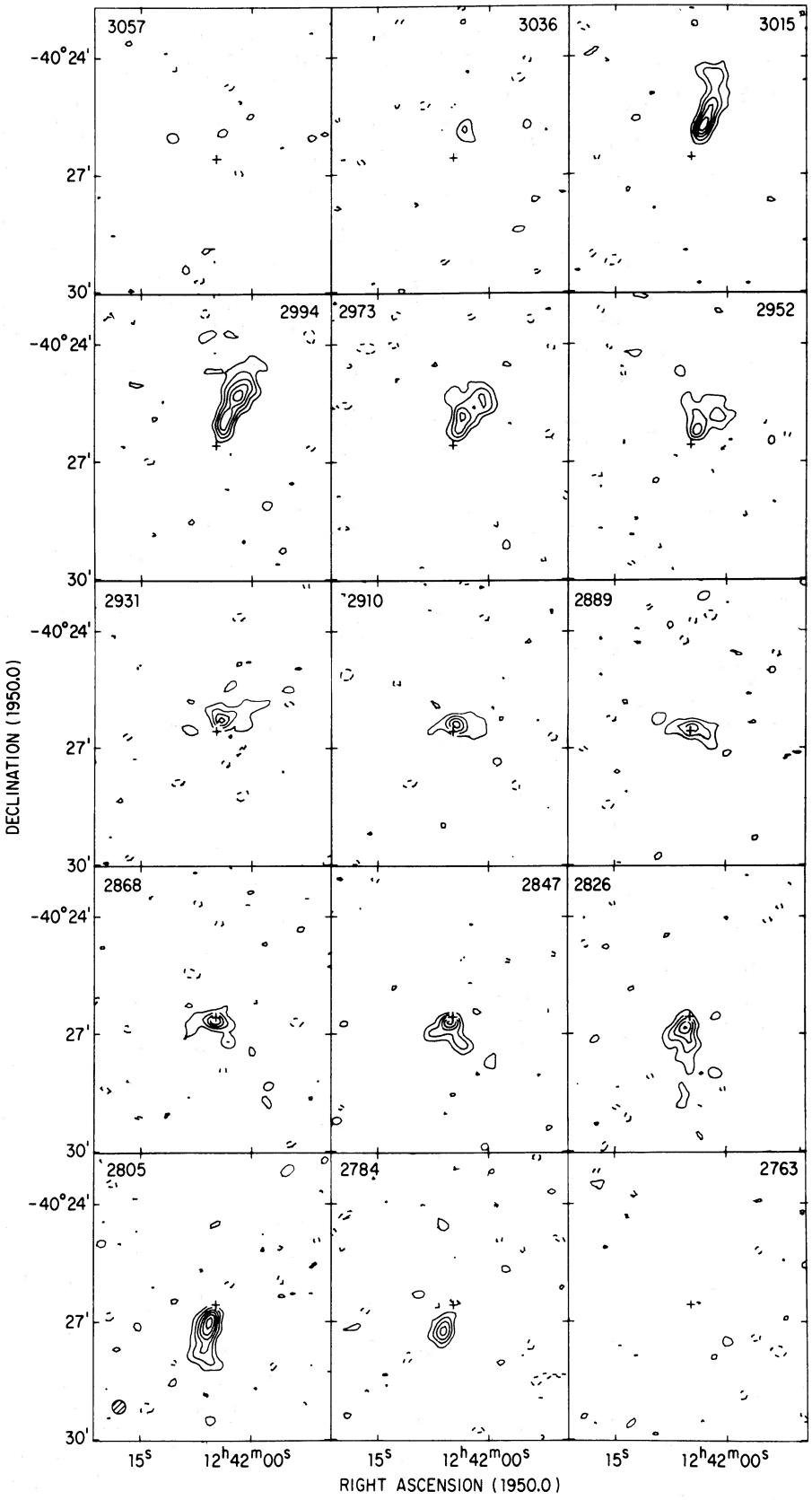

FIG. 6.—Channel maps for NGC 4650A, with contours of 3 mJy per beam

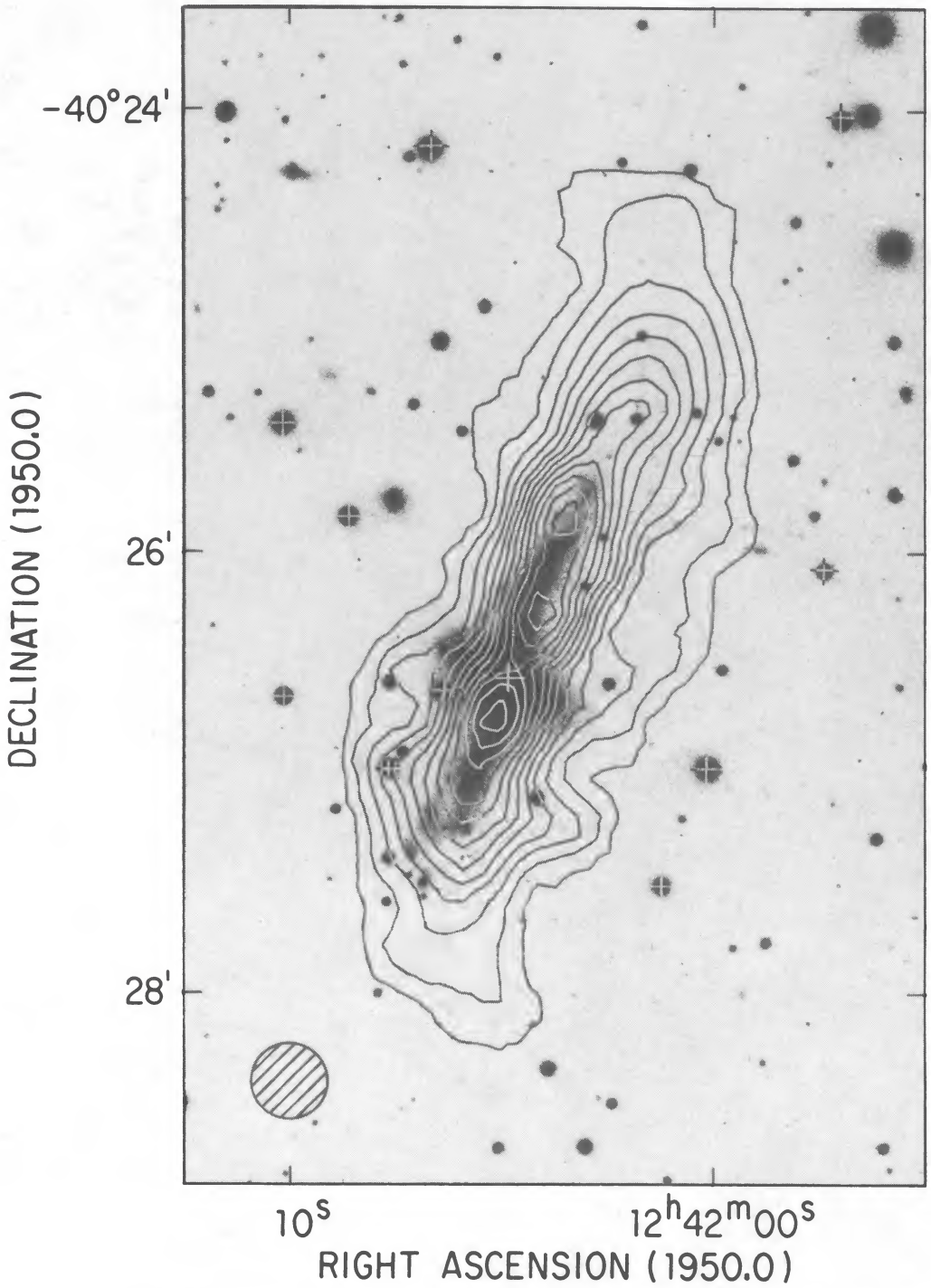

FIG. 7.—Hydrogen contours for NGC 4650A, superposed on a reproduction of a IIIa-J plate taken at the prime focus of the Cerro Tololo 4 m telescope. Contours are in steps of 2.9×10^{20} atoms cm^{-2}.

tion. Laustsen and West (1980) give a radius for the ring of roughly 45″. Beyond it, they identify faint "wisps" extending 80″ to the south of the nucleus and 100″ to the north. The H I in Figure 7 extends 100″ to the south of the nucleus and 144″ to the north. Star formation would therefore seem to be confined to the inner parts of the H I.

While the observed asymmetry, irregularity, and warping, both in the optical and in H I, might be taken as evidence for the relatively recent formation of the polar ring, they might also be taken as signs of a recent interaction with a neighboring galaxy. NGC 4650 lies only a few diameters away, has a redshift close to that of NGC 4650A, and is itself somewhat peculiar in the openness of the spiral arms originating at the ends of its bar (see Laustsen and West (1980), Fig. 1).

VII. MGC −5-7-1

a) H I *Emission*

The peculiar nature of this galaxy was first noted by Arp and Madore; it is cataloged as AM 0226−32 in their *Catalogue of Southern Peculiar Galaxies* (1986). Among polar ring systems, it is most like IC 1689, in that both have narrow rings which

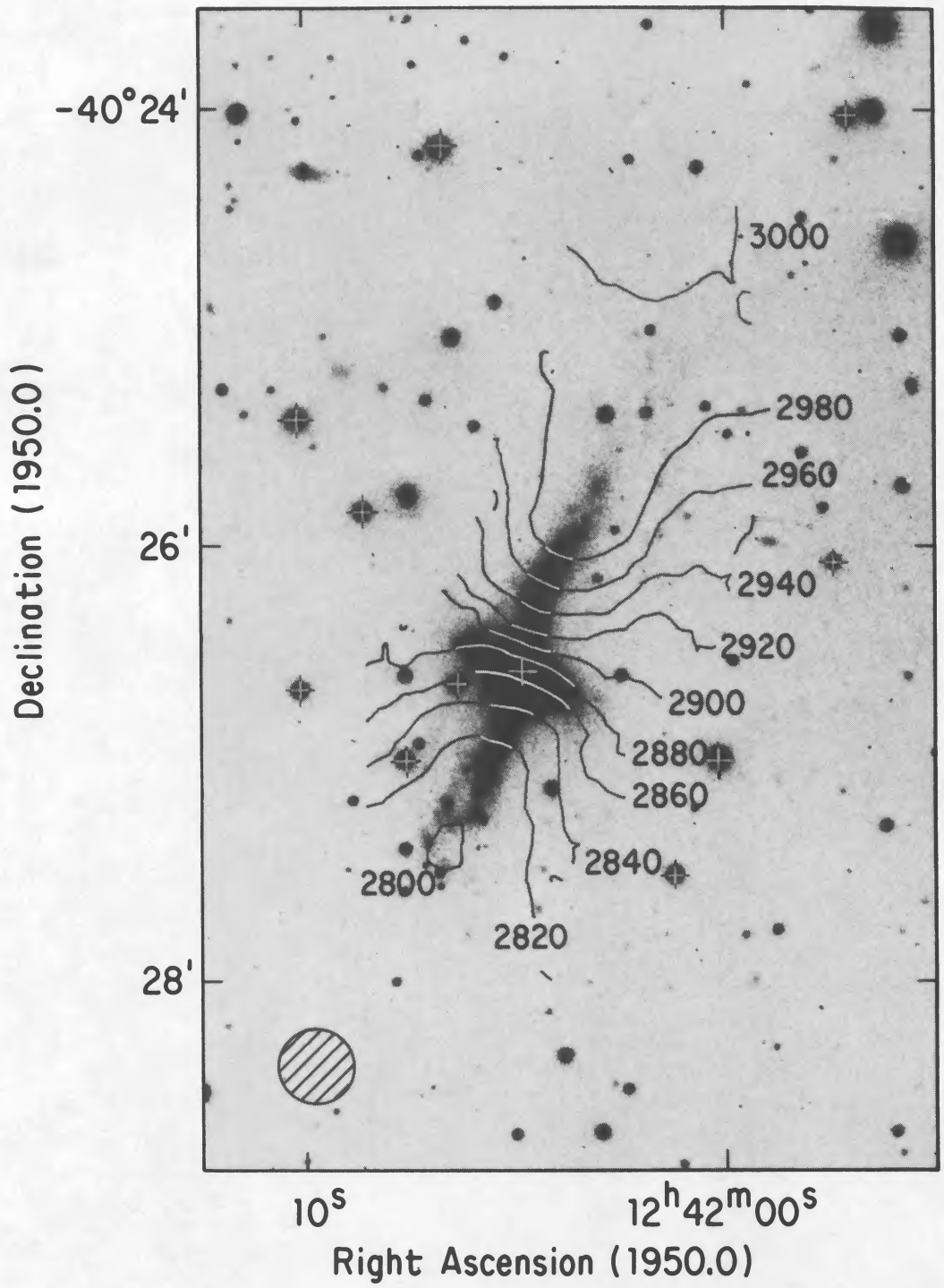

FIG. 8.—Mean H I velocities for NGC 4650A

are smaller than their associated S0's and very much less luminous. There are further similarities in that the outer isophotes are disturbed, and there is weak [O III] emission in the nucleus in both cases.

Total hydrogen contours are plotted in Figures 11*a* and 11*b*, superposed on images obtained from a 30 minute exposure with a Texas Instruments CCD and a Gunn *r* filter. The contrast on these has been adjusted to emphasize the faint outer features in the optical images. Contours of constant velocity are shown in Figure 12, superposed on an image produced from the same CCD frame, but at lower contrast emphasizing the polar ring. A position-velocity diagram, taken through the center of the galaxy at a position angle of 90°, is shown in Figure 13. This figure was derived using only the data from the B-C array, with its full velocity resolution. A global H I profile is shown in Figure 14. Integrating over velocity yields a total H I mass of $1.8 \times 10^9 M_\odot$. Channel maps are shown in Figure 15.

The H I is asymmetric, with column densities roughly twice as high in the east as in the west, and with the central peak offset to the east of the optical center (see Fig. 9 in Schechter, Kristian, and van Gorkom 1985). The total H I contours are

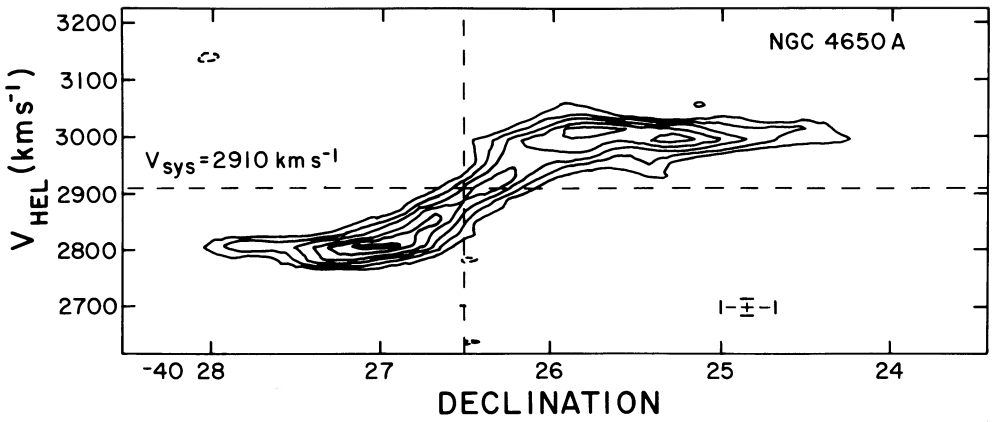

FIG. 9.—Position-velocity diagram for NGC 4650A

rounder than the optical ring, extending at least a factor of 2 beyond it and exhibiting a butterfly-like shape.

The velocity structure of the system is likewise asymmetric. Taking the mean of the extreme velocities in Figure 13, we compute $V_{sys} = 4585$ km s^{-1}. However, the mean velocity of the gas at the center of the galaxy is 4620 km s^{-1}. The optical absorption-line redshift, which lies between these values, is too uncertain to help choose between them. Though the extreme velocities indicate rotation of order 150 km s^{-1}, the velocity asymmetry makes the precise value rather uncertain. The turnover in the position-velocity diagram of MCG −5-7-1 yields an upper limit of 20″ on the size of any possible hole in its H I distribution.

b) *Direct Images*

The direct CCD data for MCG −5-7-1 have so large a dynamic range that a single photographic representation fails to convey all the information contained. Windowing the data to produce a low-contrast image of the system, Figure 16 (*upper panel*), shows the polar ring in absorption against the central S0, and makes it clear that the central component is indeed an S0 and not an elliptical.

Higher contrast images produced from the same data (Figs. 11*a*, *b*, and 16) show optical features—loops, arcs, and shells—of the sort which are frequently taken (Toomre 1977; Quinn 1984) to be evidence of recent mergers between galaxies. While there are significant differences between these faint outer features and the H I contours, the similarities suggest a common origin. We note that the direction of the gradient in the inner H I lies, to within the uncertainties, along the major axis of the ring.

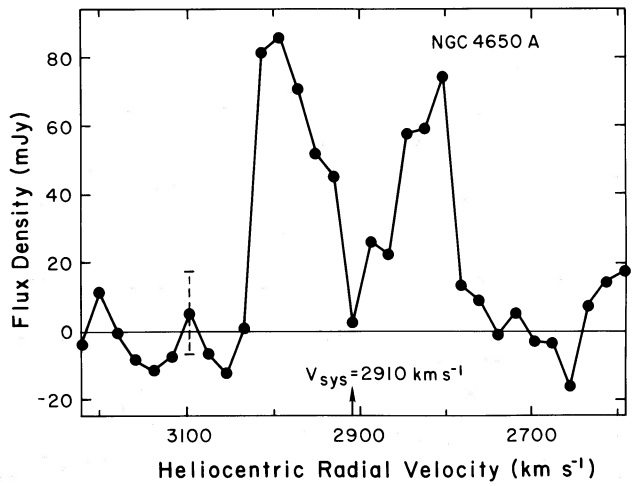

FIG. 10.—Global H I profile for NGC 4650A

For the sake of argument, we adopt the hypothesis that the optical ring, the outer features, and the irregular hydrogen are all the products of a recent merger of a galaxy with the central S0. The merger must have occurred within the last few orbital times, since neither the optical features nor the hydrogen, both of which we take to be debris from a disrupted galaxy, have settled into an equilibrium configuration. Nonetheless, there has been time enough for at least some of the hydrogen to have formed a ring and to have begun forming stars.

A possible objection to the merger picture for the formation of this system is the fact that the H I appears to be somewhat more extended than the stellar debris (though this depends upon which of the apparent features one discounts as artifacts introduced by imperfect correction for the response of the CCD). Since the stellar component of the disrupted galaxy cannot lose energy, while the gaseous component can, we would expect the gaseous component to be more tightly bound than the stellar component. Gunn (1982) has made this argument against the broader hypothesis that disks, in general, form as the result of mergers. For the case of MCG −5-7-1, we would note by way of rebuttal first, that most of the gas has not yet had time to settle, and second, that there is a well-established tendency for the ratio of H I to stellar luminosity to increase with increasing radius in disk systems. The gaseous component would therefore, on average, be torn from the disrupted galaxy earlier in the merger process than the stellar component. The outermost features in Figure 11*b* are at the limit of detectability. It may be that fainter yet features lie farther from the system.

c) *Orientation of the Ring*

The position angles of the S0 and the ring are 17°.3 and 94°.2, respectively, giving a projected angle between the two of 76°.9. The axial ratio of the ring is 0.38, implying an inclination to the line of sight of 68° if the ring is circular. The S0 appears to be nearly edge-on. We obtain a very conservative lower limit of 71° for its inclination to the line of sight by fitting ellipses to its isophotes and taking the inverse cosine of the minimum ellipticity.

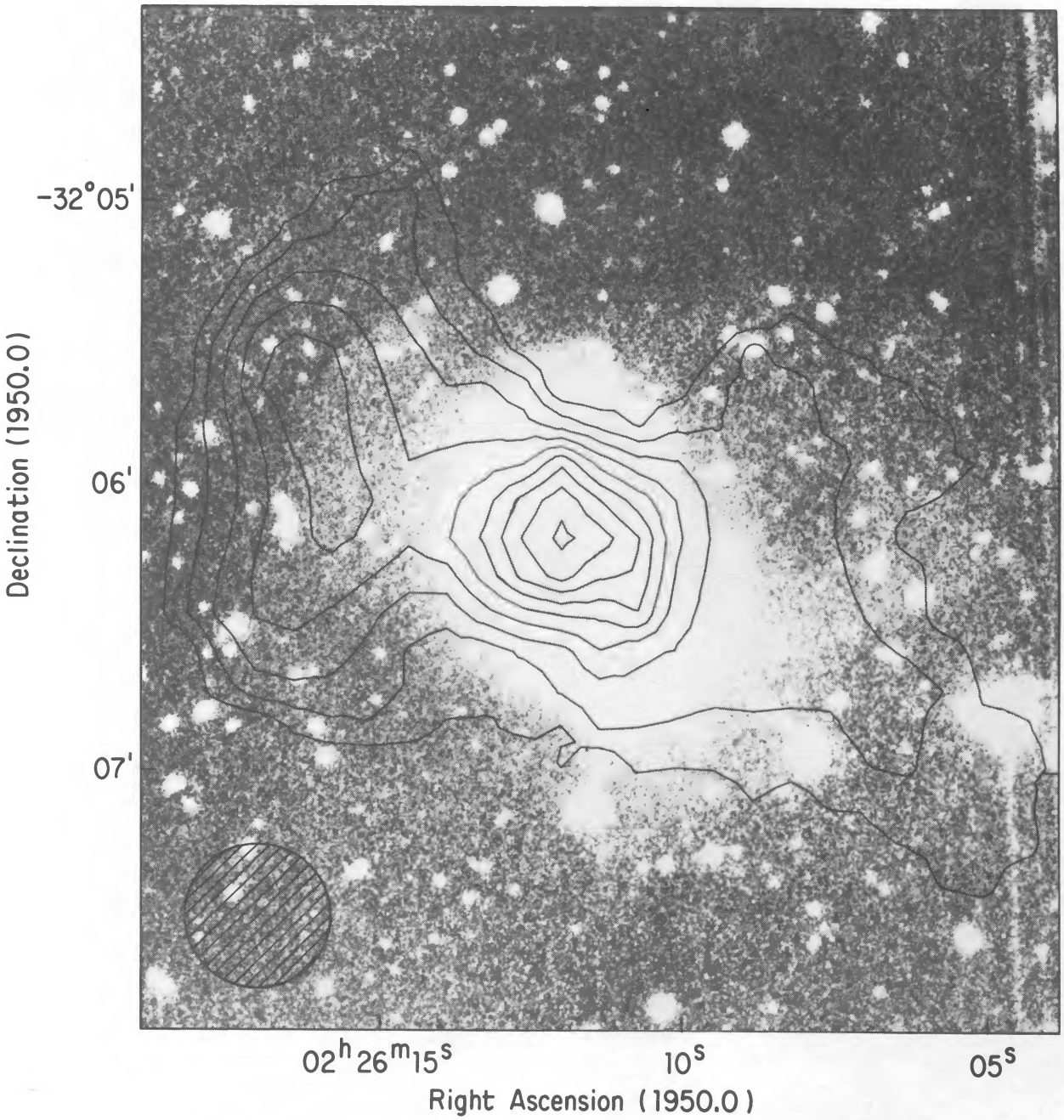

FIG. 11*a*.—Hydrogen contours for MCG −5-7-1, superposed on an image produced from a 30 minute *r* exposure with a TI CCD, obtained with the du Pont 2.5 m telescope. Contours are in steps of 6.3×10^{19} atoms cm^{-2}.

Following the approach developed by Whitmore (1984), and using our lower limit for the inclination of the S0, we find that the intrinsic angle between the ring and the S0 is either 85°.7 or 71°.2. If the S0 is more nearly edge-on, the two solutions converge toward the projected angle between the two components, 76°.9. While the deviation from orthogonality is small, the observations are inconsistent with the hypothesis of a circular ring orthogonal to the S0.

One can always, however, find an orthogonal ring by dropping the constraint that it be circular, even if one imposes the additional constraint that one of the ring's principal axes must lie along the pole of the S0. For an S0 inclination of 71°, we find (see Appendix A) that we can match the observations with an elliptical ring with axial ratio 0.66, but with the *short* axis of the ellipse aligned with the pole of the S0. This runs counter to our expectation (see Richstone 1982, Fig. 17) that the *long* axis of the ring should be aligned with the pole, and strikes us as rather improbable. The axis ratio for the ring becomes yet more extreme as the inclination of the S0 approaches 90°.

Under the merger hypothesis, the plane of the ring should coincide with the orbital plane of the recently cannibalized companion and would have no preferred orientation with respect to the S0. The alignment of the ring with the H I velocity field lends some credence to this interpretation.

d) The Blue Companion

On first mapping MCG −5-7-1 using data obtained with the C-D hybrid array, we found that the H I contour at 4583 km s^{-1} lay very close to the faint blue galaxy 52″ to the south. Suspecting that this might be the remnant of a system

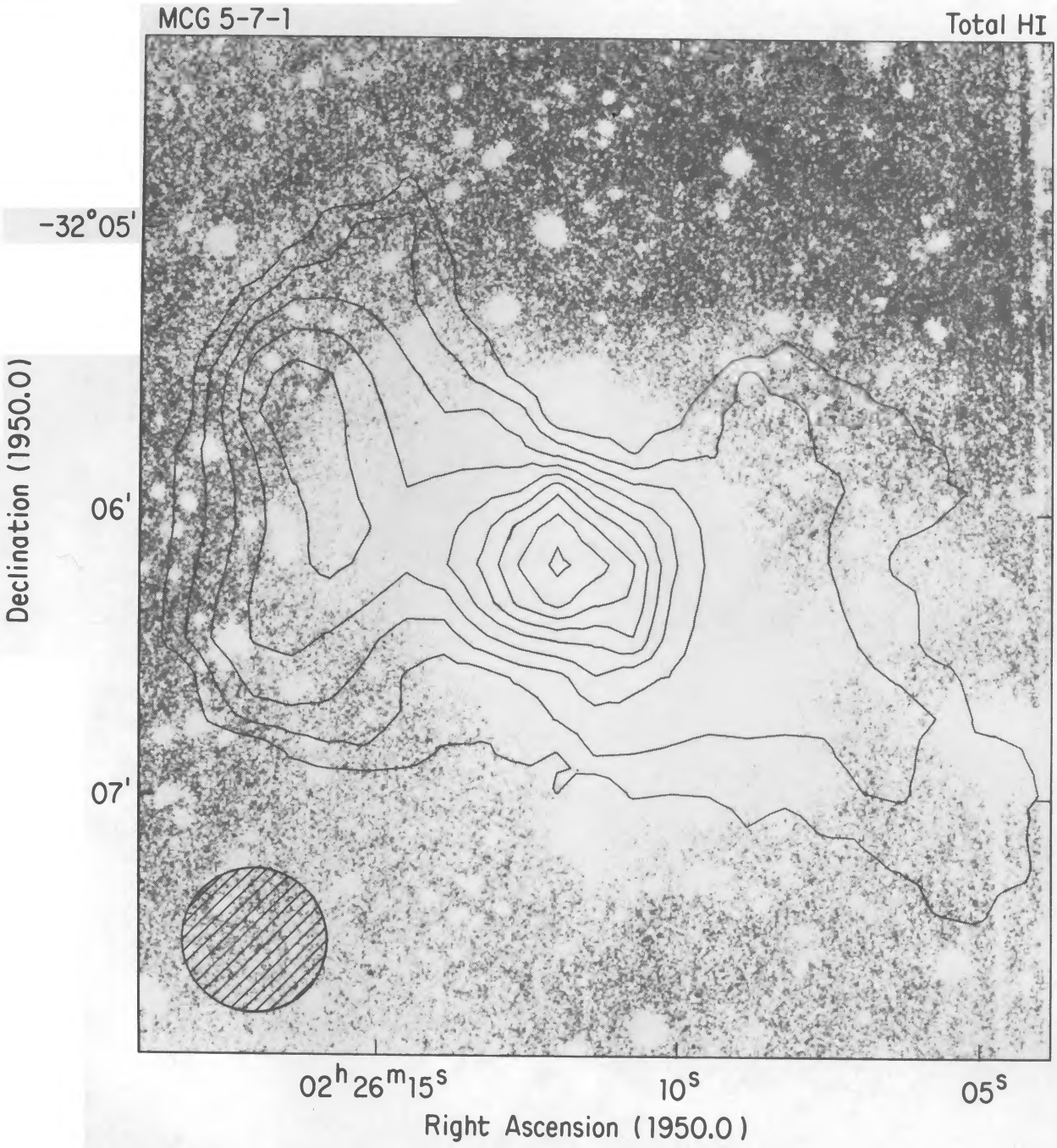

FIG. 11*b*.—Hydrogen contours as in Fig. 11*a*, but superposed on a higher contrast image

destroyed in an encounter with MCG −5-7-1, we obtained an optical spectrum at Las Campanas, which showed emission from [O II] at λ3727, [O III] at λ5007 and λ4959, and Hβ. It also showed calcium H and K absorption lines, and some evidence for absorption at the positions of Hδ and Mg *b*. The redshift for all of these was 29,860 km s^{-1}. We subsequently found that the contours at 4583 km s^{-1} obtained with B-C hybrid array did not lie close to the blue companion.

We have often heard the claim that discrepant results are left lying in desk drawers, either in a deliberate attempt to suppress evidence for "nonvelocity redshifts," or as an expression of a less malicious inclination to disregard discordant results. While we doubt that there will ever be a testable hypothesis about the circumstances under which and frequency with which nonvelocity redshifts can be expected to appear, we draw attention to our result for the blue galaxy to the south so as not to deny our colleagues data which might conceivably help them to make their case.

VIII. DISCUSSION—POLAR RINGS AS A CLASS

Schweizer, Whitmore, and Rubin (1983) have demonstrated that polar ring galaxies are encountered sufficiently often to warrant their study as a class rather than as unrelated individual objects. They address several outstanding issues, including the mechanism and frequency of formation, ages, and the shapes of the underlying potentials.

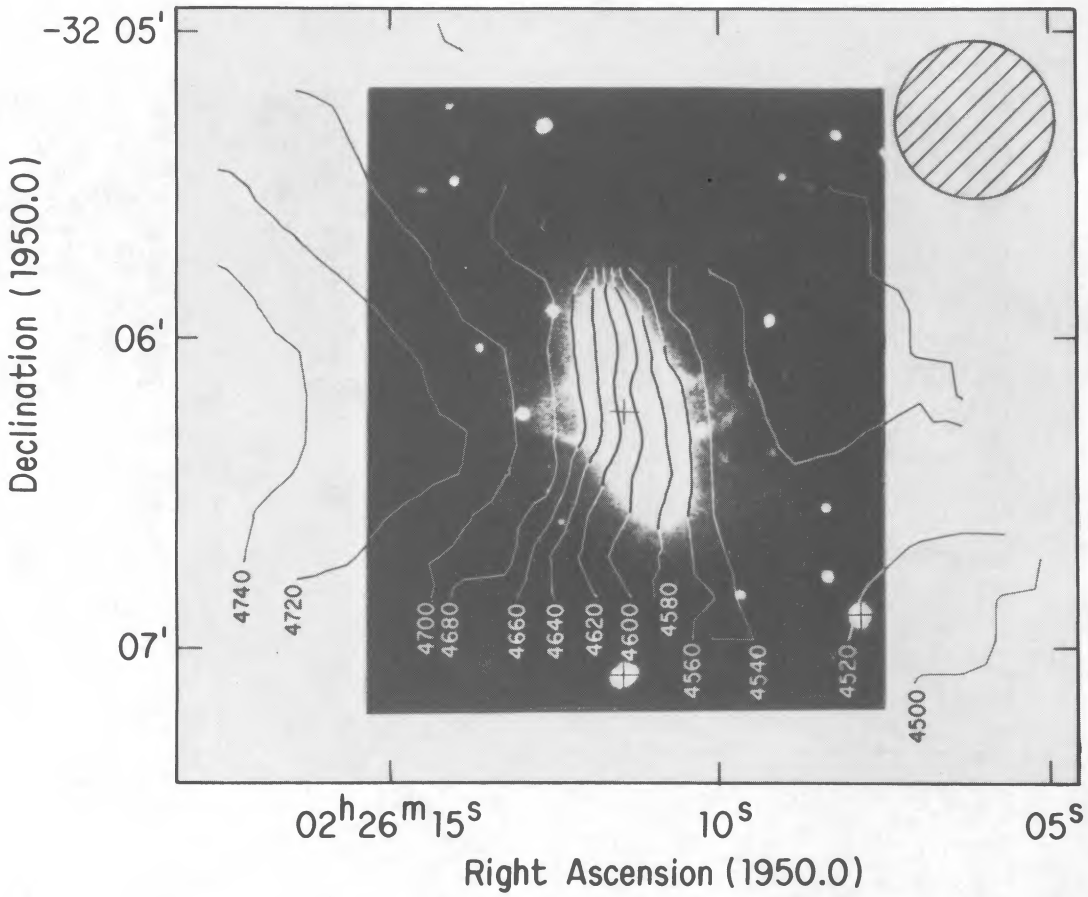

FIG. 12.—Mean velocities for MCG −5-7-1

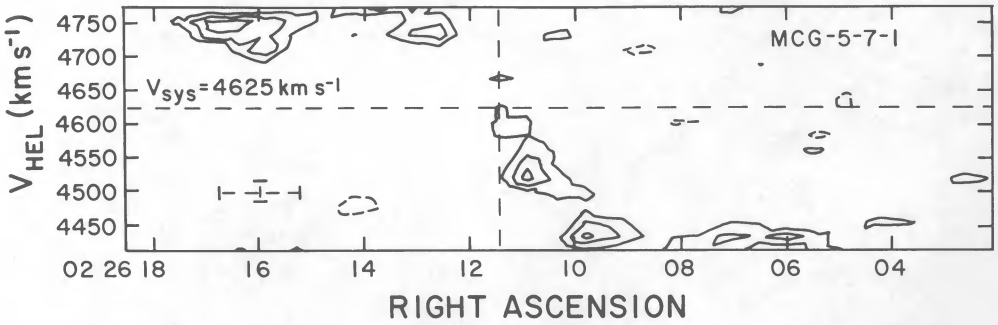

FIG. 13.—Position-velocity map for MCG −5-7-1, computed using only B-C array data at full velocity resolution

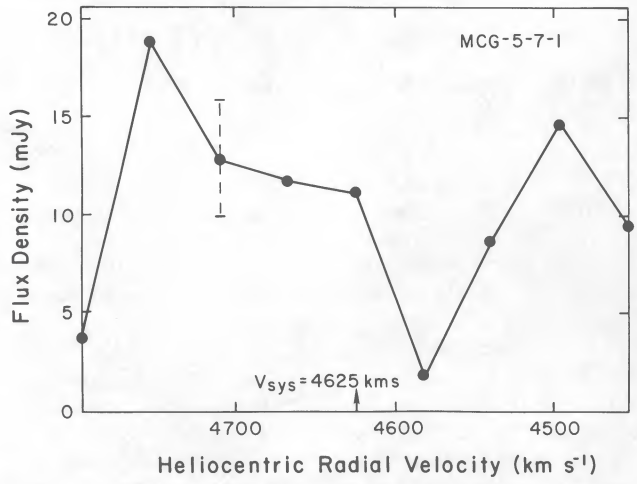

FIG. 14.—Global H I profile for MCG −5-7-1

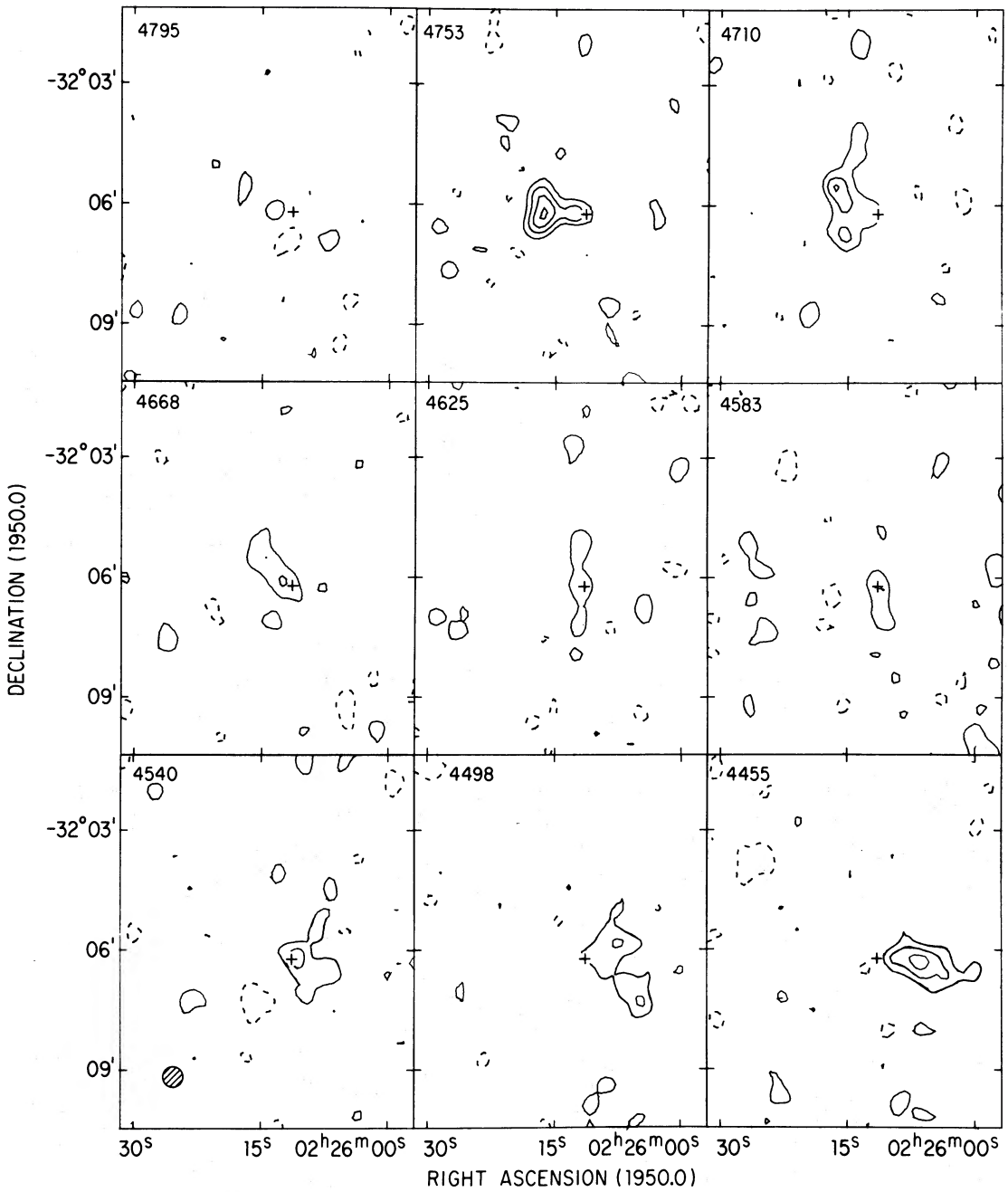

FIG. 15.—Channel maps for MCG −5-7-1, with contours of 1 mJy per beam

a) Formation Mechanism

All of the proposed mechanisms for the formation of polar rings involve the accretion of new material following the formation of the central S0. These include the complete cannibalization of a companion galaxy, the partial accretion of material from a neighbor, and the accretion of a gas cloud (as distinct from a galaxy).

The complete cannibalization of a companion seems likely in the case of MCG −5-7-1, where we see arcs, filaments, and perhaps shells, which we take to be stellar debris from the unfortunate victim.

In two cases, II Zw 73 and NGC 4650A, there are nearby, distorted companions, which might argue for mass transfer rather than a complete merger. Other systems (i.e., NGC 2685, MCG −5-7-1, UGC 7576, IC 1689, and A0136−0801) would appear to be relatively isolated, but the counterargument is strong only in the cases of NGC 2685 and MCG −5-7-1, which appear to be relatively young.

b) Ages

One can make a crude ordering of the six polar rings detected in H I, based on the regularity of the neutral hydrogen. The systems A0136−0801 and UGC 7576 would rank equally as the most regular, followed by II Zw 73. NGC 4650A is much more irregular than these, with NGC 2685 and MCG −5-7-1 more irregular yet. The time scale for the smoothing

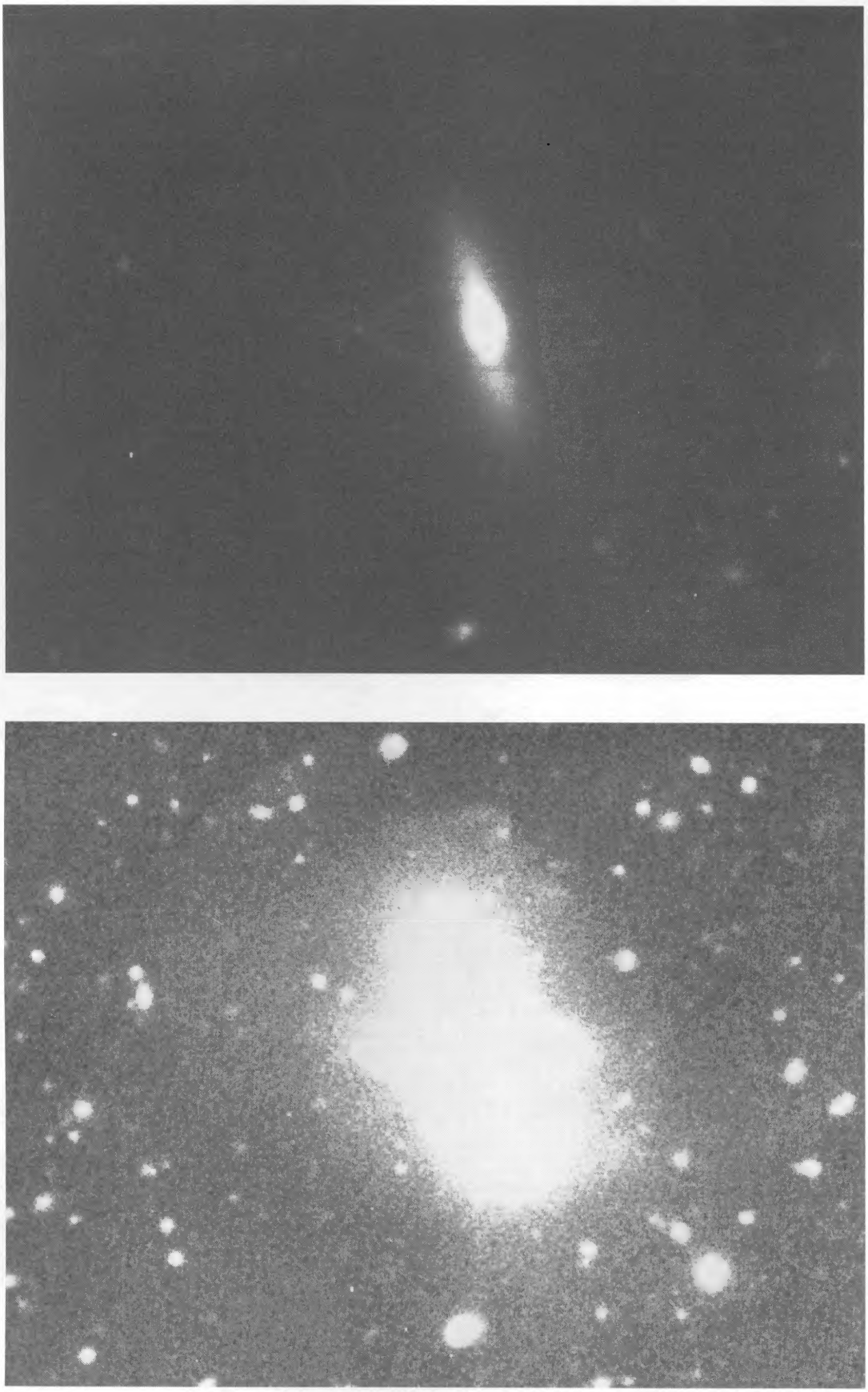

FIG. 16.—Images of MCG −5-7-1, with contrast adjusted to emphasize absorption by dust in the ring and the lenticular nature of the central component (*upper panel*) and optical arcs and filaments at intermediate distances from the SO (*lower panel*).

out of neutral hydrogen in an orbital plane must be, to within a constant, the orbital time multiplied by the ratio of the circular velocity to the typical random velocity. Since this last factor is typically of order 10, while the ratio of the Hubble time to the orbital time is more typically 100, it would seem that at least three of our systems are the results of relatively recent events.

To the extent that optical data can be brought to bear on the question of ages, they tend to bear out both the ordering and the time scales deduced from the H I. In particular, the stellar debris in the vicinity of MCG −5-7-1 would argue for an age of no more than a few orbital times. The irregular appearance of the ring and wisps in NCG 4650A would indicate ages only slightly larger. By contrast, the regular appearance of the optical rings in UGC 7576 and A0136−0801 (and to a lesser extent, II Zw 73), coupled with the coincidence of the optical emission with neutral hydrogen, would indicate more evolved systems.

c) *Stability*

Several mechanisms have been suggested to explain the apparent stability of polar ring systems. These would include (*a*) a stationary triaxial potential (Steiman-Cameron and Durisen 1982), (*b*) a tumbling prolate or triaxial potential (van Albada, Kotanyi, and Schwarzschild 1982), and (*c*) the self-gravity of the ring itself (Sparke 1986). It may be that different mechanisms are at work in different systems.

NGC 2685, MCG −5-7-1, and to a lesser extent, NGC 4650A, would appear to be, by virtue of their optical appearance and asymmetric H I, relatively young. The polar rings in these systems may be transient, in which case there is no need for a stabilizing mechanism.

Among those systems which look older, the distinction between those which are very nearly polar and those which are less so may be an important one. The rings in IC 1689 and A0136−0801 are so nearly perpendicular to the central S0's that even a small degree of triaxiality would suffice to render them stable. Even if the potentials are truly oblate, the time scales for differential precession are long: comparable to, and perhaps exceeding the Hubble time.

The time scales for differential precession are likely to be shorter in the cases of UGC 7576 and II Zw 73. Yet their neutral hydrogen maps and optical images appear to be relatively symmetric. In both cases the H I and optical images coincide, indicating that star formation has taken place throughout the H I disk. The argument for their relative youth, based on the ratios of H I to optical luminosity, is not entirely persuasive.

Of the mechanisms which might stabilize these two, a tumbling potential would require greater warping than a self-gravitating ring, with the deviation from orthogonality varying roughly linearly with radius. This would appear to be ruled out by H I and optical observations. Making plausible assumptions about the shapes of the underlying potentials, Sparke (1986) has argued that there is enough H I observed in UGC 7576 and II Zw 73 for self-gravity to stabilize their rings. To the extent that the stars observed in the rings contribute to its mass, the argument is strengthened. This argument is weakest, and hence most easily tested, in the requirement that the rings not span too great a range of radius. Both hypotheses could be subjected to further tests.

The difference between the hypothesis of a stationary triaxial potential and that of a self-gravitating ring is more than one of degree. Under the self-gravitating ring hypothesis, the ring precesses about the pole of the S0. Under the triaxial potential hypothesis, the ring would precess about one of the other two axes, eventually settling into a polar orbit.

d) *Frequency*

The difficulties in estimating the frequency with which polar ring systems form are formidable (Schweizer, Whitmore, and Rubin 1983). One must account for the probability of identifying a system as a polar ring and for the ages of the rings. Both of these are difficult to estimate. More interesting and more difficult still would be an extrapolation from the case of polar rings to the case of equatorial rings. If some rings form perpendicular to the disks of the S0's, others must form in the same plane; indeed one might expect this to be the more likely outcome of the typical galaxy merger. Such a galaxy would be difficult to distinguish from an ordinary spiral, though one can point to several candidates (Schweizer *et al.* 1986).

We thank our many colleagues who have obtained and generously contributed data to help us in the course of this program: E. Danielson, R. Giovanelli, R. Lynds, F. Schweizer, S. E. and K. M. Strom, K. Wakamatsu, and R. West. We thank J. Tonry and S. Tremaine for helpful conversations, L. Sparke for communicating results in advance of publication, and A. Toomre for communicating results in lieu of publication. NRAO is operated by Associated Universities, Inc., under contract to the National Science Foundation. This work was supported in part by NSF grant RO-8503097 to Princeton University.

APPENDIX A

PROJECTED ELLIPTICAL RINGS: INTRINSIC AXIAL RATIOS AND INCLINATIONS TO THE LINE OF SIGHT

In discussing MCG −5-7-1, we considered the possibility that we knew the projected axial ratio of an ellipse, the angle between its projected major axis and the projection of its intrinsic major axis onto the sky, and the inclination of the intrinsic axis to the plane of the sky. We wished to solve for the intrinsic axial ratio and the inclination of the plane of the ellipse to the line of sight. In our search of the literature, we were unable to locate a solution to this problem, nor were the colleagues we consulted able to point to one. We therefore proceeded to solve the problem for ourselves, and present it here for the convenience of the reader.

The problem is illustrated in Figure 17, where the x and y axes of the unprimed frame coincide with the intrinsic axes of the ellipse, OA and OB. The double primed frame is that of the sky, with the z'' axis along the line of sight and the x'' axis coincident with the intersection of the plane of the ellipse and that of the sky. The x' and y' axes of the primed frame lie in the plane of ellipse, but they have been rotated so that the x' axis also coincides with the intersection of the plane of the ellipse and that of the sky.

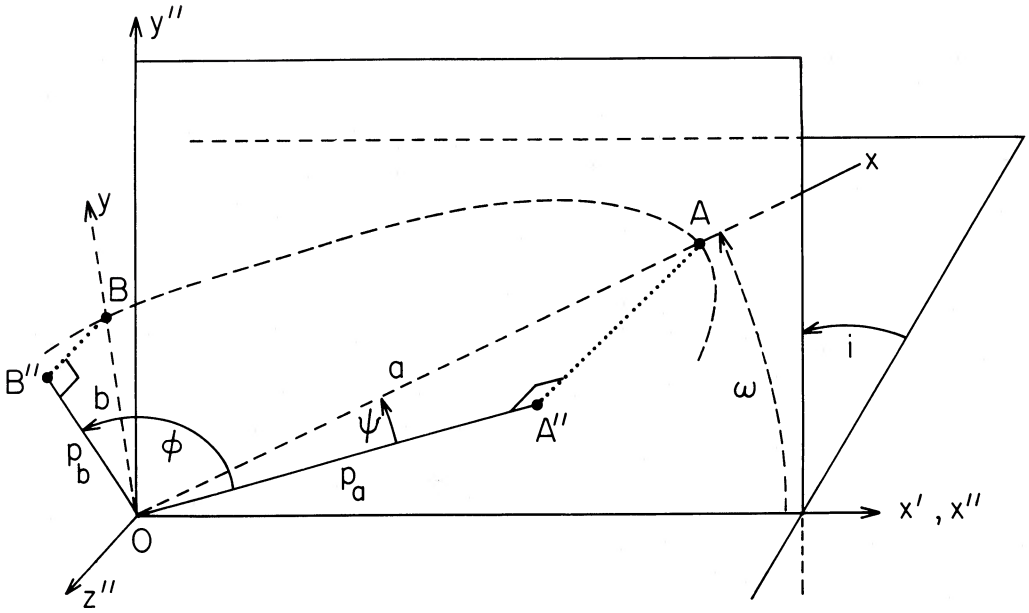

FIG. 17.—The ellipse denoted by the dashed line through A and B lies in the (x-y)-plane, which is inclined at angle i to the (x''-y'')-plane. The major axis OA projects onto OA″, and the minor axis OB projects onto OB″. The angle ϕ between the projections of the major and minor axes is not, in general, a right angle.

The intrinsic major axis of the ellipse, OA, makes an angle ω with the x' axis. The plane of the sky is inclined by angle i to the plane of the ellipse. The x'' and y'' coordinates of a point in the (x, y)-plane are given by

$$x'' = (x \cos \omega - y \sin \omega) \tag{A1}$$

$$y'' = (x \sin \omega + y \cos \omega) \cos i \, . \tag{A2}$$

If we denote the projections of the major and minor axes onto the plane of the sky by $\boldsymbol{p}_a$ and $\boldsymbol{p}_b$, then we find

$$\boldsymbol{p}_a \cdot \boldsymbol{p}_b = -ab \sin \omega \cos \omega \sin^2 i \tag{A3}$$

$$|\boldsymbol{p}_a|^2 = a^2(1 - \sin^2 \omega \sin^2 i) \tag{A4}$$

$$|\boldsymbol{p}_b|^2 = b^2(1 - \cos^2 \omega \sin^2 i) \, . \tag{A5}$$

For the case of MCG −5-7-1, we assume that the intrinsic major axis of the ring coincides with the pole of the S0 (as it turned out, we found $a < b$, indicating that the minor axis coincided with the pole). Letting ψ be the angle between plane of the sky and the major axis of the ellipse, we have $|\boldsymbol{p}_a| = a \cos \psi$, which yields

$$\sin \omega = \sin \psi / \sin i \, . \tag{A6}$$

We use equation (A6) to eliminate ω from our equations. The square of the cosine of the angle ϕ between the projections of the major and minor axes, $\boldsymbol{p}_a$ and $\boldsymbol{p}_b$, and the ratio of the squares of the projections are then given by

$$\cos^2 \phi = \tan^2 \psi [(\sin^2 i - \sin^2 \psi)/(1 + \sin^2 \psi - \sin^2 i)] \tag{A7}$$

and

$$|\boldsymbol{p}_a|^2/|\boldsymbol{p}_b|^2 = (a^2/b^2) \cos^2 \psi/(1 - \sin^2 i + \sin^2 \psi) \, . \tag{A8}$$

The projection $\boldsymbol{p}_a$ of the intrinsic major axis is taken as known. The projection $\boldsymbol{p}_b$ of the intrinsic minor axis can be obtained either by construction (Smart 1977, Fig. 130) or analytically. We proceed analytically, letting θ be the angle between the projection of the intrinsic major axis and the projected major axis, and defining $\eta = (a''^2 - b''^2)/(a''^2 + b''^2)$, where a'' and b'' are the respective lengths of the projected major and minor axes. We solve for the angle between the two projections and their ratio, finding

$$\cos^2 \phi = (\eta^2 \sin^2 2\theta)/(1 + \eta^2 - 2\eta \cos 2\theta) \tag{A9}$$

and

$$|\boldsymbol{p}_a|^2/|\boldsymbol{p}_b|^2 = (1 - \eta \cos 2\theta)^2/(1 + \eta^2 - 2\eta \cos 2\theta) \, . \tag{A10}$$

The angle θ is the complement of the angle between the major axis of the projected ellipse and that of the S0. The parameter η is readily calculated from the observed axial ratio of the projected ellipse, and the angle ψ is known from the inclination of the S0. We can therefore solve equations (A7) and (A9) for the inclination i of the ring to the line of sight. We can then solve equations (A8) and (A10) for the intrinsic axial ratio, b/a.

REFERENCES

Arp, H., and Madore, B. M. 1986, *Catalogue of Southern Peculiar Galaxies and Associations* (Cambridge: Cambridge University Press), in press.
Gunn, J. E. 1982, in *Astrophysical Cosmology*, ed. H. A. Brück, G. V. Coyne, and M. S. Longair (Vatican City: Pontifical Academy of Sciences), p. 223.
Högbom, J. A. 1974, *Astr. Ap. Suppl.*, **15**, 417.
Lauberts, A. 1984, *Astr. Ap. Suppl.*, **58**, 249.
Laustsen, S., and West, R. M. 1980, *J. Ap. Astr.*, **1**, 177.
Quinn, P. J. 1984, *Ap. J.*, **279**, 596.
Richstone, D. O. 1982, *Ap. J.*, **252**, 496.
Richstone, D. O., and Potter, M. D. 1982, *Nature*, **298**, 728.
Schechter, P. L., and Gunn, J. E. 1978, *A.J.*, **83**, 1360.
Schechter, P. L., Kristian, J., and van Gorkom, J. H. 1985, *Ann. Rep. Dir. Mt. Wilson and Las Campanas Obs., 1984–1985*, p. 33.
Schechter, P. L., Sancisi, R., van Woerden, H., and Lynds, C. R. 1984, *M.N.R.A.S.*, **208**, 111.
Schechter, P. L., Ulrich, M.-H., and Boksenberg, A. 1984, *Ap. J.*, **276**, 526.
Schweizer, F., Ford, K., Giovanelli, R., and Jedrzejewski, R. I. 1986, private communication.
Schweizer, F., Whitmore, B. C., and Rubin, V. C. 1983, *A.J.*, **88**, 909.
Sersic, J. L. 1967, *Zeitschrift für Astrophysik*, **67**, 306.
Shane, W. W. 1980, *Astr. Ap.*, **82**, 314.
Smart, W. M. 1977, *Textbook on Spherical Astronomy*, (6th ed.; Cambridge: Cambridge University Press), p. 352.
Sparke, L. S. 1986, *M.N.R.A.S.*, **219**, 657.
Steiman-Cameron, T. Y., and Durisen, R. H. 1982, *Ap. J. (Letters)*, **263**, L51.
Thuan, T. X., and Gunn, J. E. 1976, *Pub. A.S.P.*, **88**, 991.
Thompson, A. R., Clark, B. G., Wade, C. M., and Napier, P. J. 1980, *Ap. J. Suppl.*, **44**, 151.
Tohline, J. E., Simonson, G. F., and Caldwell, N. 1982, *Ap. J.*, **252**, 92.
Toomre, A. 1977, in *The Evolution of Galaxies and Stellar Populations*, ed. R. B. Larson and B. M. Tinsley (New Haven: Yale University Observatory), p. 401.
van Albada, T. S., Kotanyi, C. G., and Schwarzchild, M. 1982, *M.N.R.A.S.*, **198**, 303.
Whitmore, B. C. 1984, *A.J.*, **89**, 618.

JEROME KRISTIAN and PAUL L. SCHECHTER: Mount Wilson and Las Campanas Observatories, 813 Santa Barbara St., Pasadena, CA 91101-1292

J. H. VAN GORKOM: NRAO, P.O. Box 0, Socorro, NM 87801